

High-Frequency and -Field Electron Paramagnetic Resonance Spectroscopic Analysis of Metal–Ligand Covalency in a $4f^7$ Valence Series (Eu^{2+} , Gd^{3+} , and Tb^{4+})

Thaige P. Gomba,[†] Samuel M. Greer,[†] Natalie T. Rice, Ningxin Jiang, Joshua Telser, Andrew Ozarowski, Benjamin W. Stein, and Henry S. La Pierre^{*}

Cite This: *Inorg. Chem.* 2021, 60, 9064–9073

Read Online

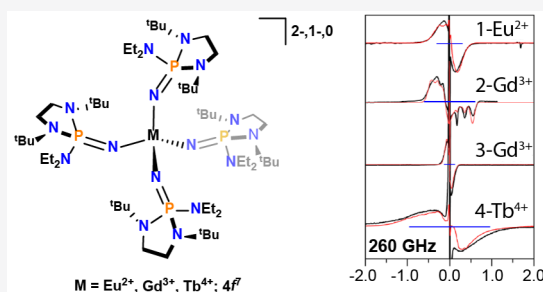
ACCESS |

Metrics & More

Article Recommendations

Supporting Information

ABSTRACT: The recent isolation of molecular tetravalent lanthanide complexes has enabled renewed exploration of the effect of oxidation state on the single-ion properties of the lanthanide ions. Despite the isotropic nature of the ^8S ground state in a tetravalent terbium complex, $[\text{Tb}(\text{NP}(\text{1,2-bis-}^t\text{Bu-diamidoethane})(\text{NEt}_2)_4)]$, preliminary X-band electron paramagnetic resonance (EPR) measurements on tetravalent terbium complexes show rich spectra with broad resonances. The complexity of these spectra highlights the limits of conventional X-band EPR for even qualitative determination of zero-field splitting (ZFS) in these complexes. Therefore, we report the synthesis and characterization of a novel valence series of $4f^7$ molecular complexes spanning three oxidation states (Eu^{2+} , Gd^{3+} , and Tb^{4+}) featuring a weak-field imidophosphorane ligand system, and employ high-frequency and -field electron paramagnetic resonance (HF-EPR) to obtain quantitative values for ZFS across this valence series. The series was designed to minimize deviation in the first coordination sphere from the pseudotetrahedral geometry in order to directly interrogate the role of metal identity and charge on the complexes' electronic structures. These HF-EPR studies are supported by crystallographic analysis and quantum-chemical calculations to assess the relative covalent interactions in each member of this valence series and the effect of the oxidation state on the splitting of the ground state and first excited state.



INTRODUCTION

The accessible molecular oxidation states of the lanthanides have rapidly expanded.^{1–4} The synthesis and characterization of novel divalent complexes has enabled a detailed understanding of lanthanide electronic structure^{5–21} and reactivity,^{22–32} and, as a result, has demonstrated significant opportunities to improve our knowledge of the magnetic properties of the lanthanides.^{33–39} Until 2019, molecular tetravalent lanthanide complexes were limited to cerium.^{40–45} Recently developed weak-field ligand systems, such as imidophosphoranes $[\text{N}=\text{P}(\text{NR}_2)_3]^-$ (R = alkyl), decrease the thermodynamic barrier for oxidation, thereby making the oxidation potential more accessible within the solvent window.^{1,2} We have recently reported the synthesis and characterization of novel lanthanide complexes featuring weak-field dialkylamide imidophosphorane ligands. This class of compounds includes the most reducing Ce^{3+} complex to date as well as one of the first isolable Tb^{4+} complexes. Similarly, the Mazzanti group has isolated a pair of Tb^{4+} complexes featuring weak-field siloxide ligands.^{43,44}

Magnetic susceptibility measurements on both the imidophosphorane- and siloxide-supported Tb^{4+} complexes demonstrate results consistent with a $4f^7$ ion formulation. Concurrent X-band electron paramagnetic resonance (EPR) measurements

resulted in broad, complex spectra that were difficult to interpret, and, thus, a quantitative evaluation of the zero-field splitting (ZFS) has not yet been possible for these molecular compounds. ZFS refers to the energetic separation between the spin projection (m_s) levels in the absence of an applied magnetic field and originates from the mixing of low-lying excited electronic states facilitated by spin–orbit coupling (SOC) and, to a lesser extent, the spin–spin coupling (SSC) of unpaired electron spins.⁴⁶ As a result, ZFS is sensitive to the interplay between the ligand field, SOC, and interelectronic repulsion and therefore offers unique insight into the ground-state electronic structures and magnetic properties. A detailed understanding of ZFS as a function of the metal identity and oxidation state in the lanthanides is a crucial reference for understanding and rationalizing the behavior of actinide $5f^7$ ions including Cm^{3+} and Bk^{4+} .^{47–50} Most importantly, this

Received: April 6, 2021

Published: June 9, 2021



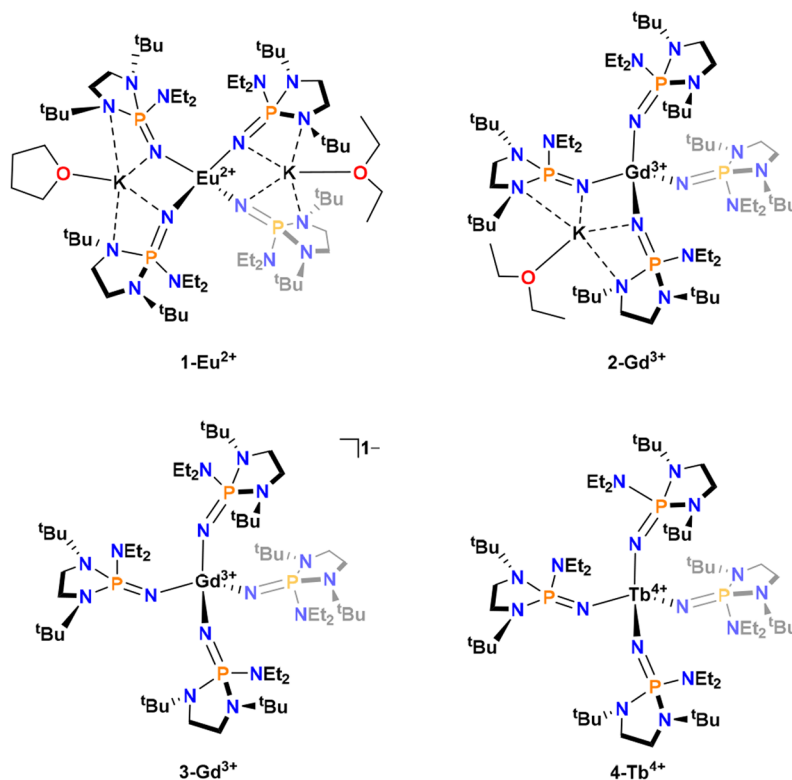


Figure 1. Molecular structures of **1-Eu²⁺**, **2-Gd³⁺**, **3-Gd³⁺**, and **4-Tb⁴⁺**. The [(2.2.2-crypt)K]⁺ was omitted in the drawing of **3-Gd³⁺** for clarity.

analysis is crucial in guiding the design principles for lanthanide single-molecule magnets, qubits, magnetocaloric effect coolants, and frustrated magnetic materials based on significant variations in the metal–ligand covalency as a function of the lanthanide oxidation state.

To address the challenge of ascertaining reliable ZFS parameters in these lanthanide systems, we have employed high-frequency and -field electron paramagnetic resonance (HFEPFR). HFEPFR has proven to be a powerful technique capable of directly determining ZFS parameters.^{51–53} To analyze the effects of oxidation state on the physical properties, we have prepared a valence series of 4f⁷ complexes consisting of Eu²⁺, Gd³⁺, and Tb⁴⁺. Herein, we report the synthesis, structural analysis, magnetic measurements, HFEPFR analysis, and quantum-chemical calculations for this imidophosphorane valence series, with the lanthanide ion spanning three oxidation states. These complexes exhibit an ⁸S ground state and, consequently, are expected to exhibit small ZFS parameters (typically |D| < ~0.1 cm⁻¹, where D is the axial, second-order ZFS^{54,55}) because of the lack of other octet states and a large separation between the ground octet and first excited sextet state.^{56–59} Until now, there has not been a series of pseudoisomeric molecular compounds of Eu²⁺, Gd³⁺, and Tb⁴⁺ to interrogate the dependence of S = 7/2 spin Hamiltonian parameters (i.e., isotropic g values and ZFS) on the metal identity and charge. The present HFEPFR studies on the Tb⁴⁺ complex demonstrate ZFS ~ 8 times greater than its closest structural analogue Gd³⁺ complex.

RESULTS AND DISCUSSION

The four homoleptic compounds investigated here are supported by the [(NP*)(1,2-bis-^tBu-diamidoethane)(NEt₂)]⁻ ligand [(NP*)]⁻^{41,42} and include [(THF)K][(Et₂O)K]-

[Eu²⁺(NP*)₄] (**1-Eu²⁺**), [(Et₂O)K][Gd³⁺(NP*)₄] (**2-Gd³⁺**), [(2.2.2-crypt)K][Gd³⁺(NP*)₄] (**3-Gd³⁺**), and the previously reported [Tb(NP*)₄]⁴¹ (**4-Tb⁴⁺**; Figure 1). The synthesis of each of these complexes is detailed in Scheme S1. All four complexes have similar primary coordination spheres with four imidophosphorane ligands coordinated in a pseudotetrahedral fashion. However, because of the interactions of the bound or unbound potassium counteranions in the second coordination sphere, both the gadolinium structures and the europium structure deviate from the S₄ point group observed in the solid-state structure of neutral **4-Tb⁴⁺**.⁶⁰ This deviation from a tetrahedral structure is quantified by two parameters in this study: (1) τ₄, where a value of 1.0 implies a perfect tetrahedral structure and a value of 0.0 implies a square-planar structure,⁶¹ and (2) Σ_{109.5}, which is the sum of the absolute difference from each of the six angles in the primary coordination sphere from the tetrahedral angle (109.5°). This latter parameter is useful because it represents absolute deviance from a tetrahedral configuration, while τ₄ represents an average deviation. As expected, the neutral complex **4-Tb⁴⁺** has a coordination geometry closest to tetrahedral of the four (τ₄ of 0.99 and Σ_{109.5} of 9.8°). In contrast, the dianionic complex **1-Eu²⁺** is furthest from a tetrahedral geometry (τ₄ of 0.82 and Σ_{109.5} of 60.6°). The two monoanionic gadolinium complexes fall in between these extremes (**2-Gd³⁺** and **3-Gd³⁺**: τ₄ of 0.94 and 0.98 and Σ_{109.5} of 28.4 and 6.0°, respectively).

The average Ln–N bond lengths are 2.483(4), 2.271(6), 2.267(4), and 2.106(3) Å for **1-Eu²⁺**, **2-Gd³⁺**, **3-Gd³⁺**, and **4-Tb⁴⁺**, respectively. The change in the bond lengths across the series follows that expected based on the six-coordinate Shannon ionic radii: Eu²⁺ (1.17 Å), Gd³⁺ (0.938 Å), and Tb⁴⁺ (0.76 Å).⁶² The average P–N_{imide} bond length [1.555(4) Å] for **4-Tb⁴⁺** is longer than those for the other compounds in

this series, which are 1.519(4), 1.521(6), and 1.523(4) Å for **1-Eu²⁺**, **2-Gd³⁺**, and **3-Gd³⁺**, respectively. This difference is greater than the error of the respective measurements but not greater than 3σ . The P–N bond lengths for **1-Eu²⁺**, **2-Gd³⁺**, and **3-Gd³⁺** are more in line with the P–N_{imide} bond lengths observed in the solid-state structure for the potassium salt of the ligand, 1.526(7) Å.⁴¹ This result could be indicative of increased electron donation to the metal center for **4-Tb⁴⁺** in comparison to **1-Eu²⁺**, **2-Gd³⁺**, and **3-Gd³⁺**.

The variable-temperature direct-current (dc) magnetic susceptibility data for all compounds in this series are shown in Figures 2 and S4–S15. All four complexes exhibit a

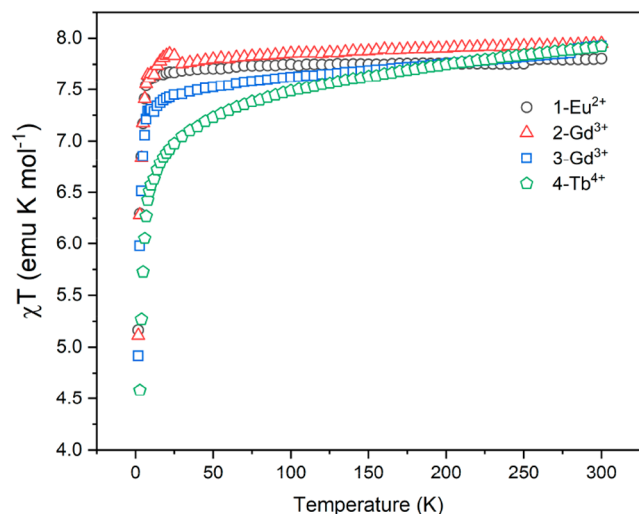


Figure 2. Variable-temperature molar magnetic susceptibility times temperature ($\chi_M T$) for **1-Eu²⁺**, **2-Gd³⁺**, **3-Gd³⁺**, and **4-Tb⁴⁺** collected under a dc field of 1 T.

consistent room-temperature $\chi_M T$ value, ranging from 7.80 to 7.93 emu·K/mol, with a theoretical value of 7.88 emu·K/mol for an isotropic $4f^7$ complex ($g = 2$, $S = 7/2$, $L = 0$, $J = 7/2$, and $\mu_{\text{eff}} = 7.94 \mu_B$). The distinguishing feature of the magnetic behavior of these compounds is their low-temperature susceptibility and is a direct result of varied ZFS parameters among these europium, gadolinium, and terbium complexes. Utilizing multifield data and accounting for increased Zeeman splitting at higher fields (see the Supporting Information, SI), the isotropic g and D values for each of these compounds can be extracted from their fit using *PHI* software (the results are summarized in Table S21).⁶³ As expected, for **1-Eu²⁺**, **2-Gd³⁺**, and **3-Gd³⁺**, the absolute values of D obtained from the fit are relatively small, ranging from 0.03(7) to 0.19(5) cm^{-1} . On the other hand, **4-Tb⁴⁺** exhibits a strikingly large $|D|$ value of 6.3(3) cm^{-1} , which is in agreement with the previously reported analyses.⁴¹

The X-band and representative HFEPR spectra of **1-Eu²⁺**, **2-Gd³⁺**, **3-Gd³⁺**, and **4-Tb⁴⁺** in solution (toluene) along with their respective simulations (using the *Matlab* toolbox *EasySpin*⁶⁴) are shown in Figure 3. The spectra of the solid-state samples and additional solution experiments along with their spectral simulations are shown in Figures S16–S19 and Table S22. All of the recorded HFEPR spectra exhibit broad linewidths away from the central transition that are indicative of strain in the ZFS parameters.^{57,65} Here, strain refers to a distribution in ZFS that results from a variation in the local coordination sphere of the molecular species under inves-

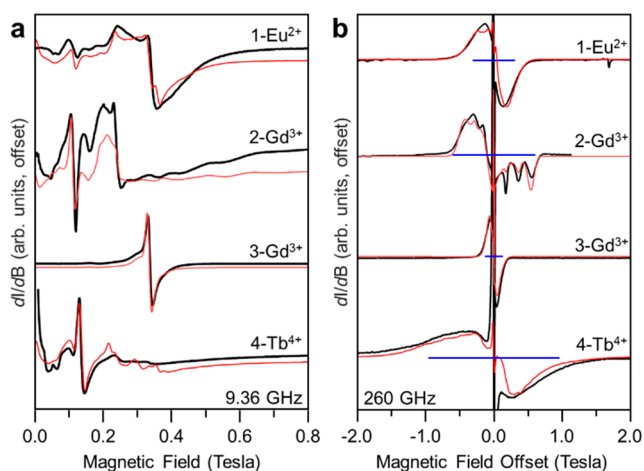


Figure 3. (a) Experimental (black traces) and simulated (red traces) X-band EPR spectra at 9.36 GHz and 5 K for **1-Eu²⁺**, **2-Gd³⁺**, **3-Gd³⁺**, and **4-Tb⁴⁺**. (b) Experimental (black traces) and simulated (red traces) HFEPR spectra at 260 GHz and 5 K for **1-Eu²⁺**, **2-Gd³⁺**, **3-Gd³⁺**, and **4-Tb⁴⁺**. The horizontal blue line represents the breadth of the feature. In these spectra, the field of the central transition is subtracted in order to facilitate a direct comparison of the observed spectral extent for each compound. Simulation parameters are given in Table 1.

tigation. This effect manifests as a broadening of the spectral features. The narrow central feature arises from the transition of $m_S = -1/2 \rightarrow m_S = +1/2$ and is, to first order, immune from the effects of strain.⁶⁶ Note that in these samples the strain is often of magnitude comparable to that of the ZFS parameter itself. This situation makes spectral simulation tedious because the often-used approximation for the effect of strain on the spectrum is strictly valid only when the strain is small compared to the central value.⁶⁴ Testing of the typical/approximate model of strain compared to an explicit model of strain showed that differences in the ZFS parameters are smaller than the estimated error in all cases except for **1-Eu²⁺** and **4-Tb⁴⁺**. For this reason, the approximate model has been employed for all compounds except for **1-Eu²⁺** and **4-Tb⁴⁺** to expedite the data analysis. The procedures for the explicit modeling of strain is detailed in the SI along with the *Matlab* script.

The EPR spectrum of a well-isolated spin ground state can be described in terms of the following spin Hamiltonian:^{54,55}

$$\hat{H}_S = \beta_e \mathbf{B} \cdot \mathbf{g} \cdot \hat{\mathbf{S}} + D \left[\hat{S}_z^2 - \frac{S(S+1)}{3} + \frac{E}{D} (\hat{S}_x^2 - \hat{S}_y^2) \right] \quad (1)$$

The first term is the electronic Zeeman interaction where β_e is the electron Bohr magneton, \mathbf{B} is the magnetic field vector, \mathbf{g} is the g tensor (assumed to be isotropic), and $\hat{\mathbf{S}}$ represents the electron spin operator. The second term describes the second-order ZFS interactions and is parametrized by D (axial term) and E (rhombic term), respectively. Here \hat{S}_μ is the component of the spin operator ($\mu = x, y, z$). Note that, in the present case where the strain is significant, there is a distribution of positive and negative D parameters.⁵⁷ In cases where $S \geq 2$, the spin system may need to be characterized by fourth-order ZFS terms, and even sixth-order terms for $S \geq 3$.^{54,55} In this work, we have limited the analysis to only second-order terms as not to overparametrize the results. In extended lattice systems containing $4f^7$ ions as dopants in high-symmetry sites, e.g., the Y^{3+} site in yttrium aluminum garnet ($Y_3Al_5O_{12}$) and the Pb^{2+}

Table 1. Spin Hamiltonian Parameters Extracted from EPR Spectroscopy of Solution Samples^a

sample	$\Sigma_{109.5}$ (deg)	g	D (cm ⁻¹)	E (cm ⁻¹)	σ_D (cm ⁻¹)	σ_E (cm ⁻¹)	Δ^8S (cm ⁻¹)	Δ^8S (cm ⁻¹) ^b
1-Eu ²⁺	60.6	1.990(5)	0.045(5)	0.008(5)	0.020	0.020	0.58	0.596
2-Gd ³⁺	28.4	1.990(5)	0.086(3)	0.018(3)	0.017	0.017	1.14	1.181
3-Gd ³⁺	6.0	1.990(5)	0.018(3)	0.005(3)	0.020	0.010	0.25	0.271
4-Tb ⁴⁺	9.8	2.010(5)	0.140(5)	0.025(5)	0.095	0.035	1.81	1.857

^aNumbers in parentheses are the estimated uncertainties in the last digit. ^bValues are calculated through first-order perturbation theory, as described in ref 72.

site in PbWO₄ (both materials have been used as hosts for Eu²⁺ and Gd³⁺)^{67–70} or thoria (host for Tb⁴⁺),⁷¹ it is possible to extract fourth- and sixth-order ZFS terms, although these are much smaller than the D ($=3B_2^0$) term. To simplify the analysis, a new parameter, Δ^8S , defined as the energetic separation between the highest and lowest m_S states of the $S = 7/2$ ground state, is employed (vide infra). This parameter is defined to capture the effect of ZFS, without the distraction that results from the ambiguity of the sign of D for a highly strained system. It corresponds to $12|D|$ at zero field for an axial system and to $[12|D| + 39.6E^2/|D|]$ for a rhombic system.⁷²

A qualitative analysis of the anisotropy of this series can be achieved by comparing the spectral extent of each compound in Figure 3b. Here, each spectrum is offset according to the resonance condition of the $\Delta m_S = \pm 1/2$ transition. This presentation allows simultaneous examination of the entire series of spectra and shows how the ZFS produces peak separations that are independent of the magnetic field (Figures S16–S19). It also allows a direct comparison of the spectral extent and thus the anisotropy of each compound (Figure 3b). Examination of Figure 3 clearly shows that the spectrum of 4-Tb⁴⁺ extends much further to either side of the central transition than in the spectra of the other compounds, indicating comparatively larger anisotropy. This expectation is confirmed by the parameters extracted from the spectral simulations (Figure 3 and Table 1), which determined that the Δ^8S parameters for 1-Eu²⁺ ($\Delta^8S = 0.58$ cm⁻¹), 2-Gd³⁺ ($\Delta^8S = 1.14$ cm⁻¹), and 3-Gd³⁺ ($\Delta^8S = 0.25$ cm⁻¹) are all significantly smaller than that of 4-Tb⁴⁺ ($\Delta^8S = 1.81$ cm⁻¹).

Additionally, the g values are isotropic and nearly equal for 1-Eu²⁺, 2-Gd³⁺, and 3-Gd³⁺ with $g = 1.990(5)$ [the g values for the free ions Eu²⁺ and Gd³⁺ are 1.9926^{73,74} and 1.991,⁷⁵ respectively]. Interestingly the g value for 4-Tb⁴⁺, $g = 2.010(5)$, is not only larger than those for the Eu²⁺/Gd³⁺ complexes but is larger than the free electron value ($g_e = 2.0023$). This unusual observation, however, is not without precedent. Although scarce, some solid-state materials containing Tb⁴⁺ have been investigated through EPR and yielded a diverse range of g values.^{71,76–78} In these cases, the g values in different host lattices span 1.997(5)–2.0146(4). The highest values were obtained in ThO₂ and ThSiO₄ host lattices, where $g = 2.0146(4)$ and 2.011(5), respectively.^{71,77} Similarly, g values for Eu²⁺ and closely related Gd³⁺ complexes exhibit a reduced g value compared to g_e .^{67,68,70,78} A qualitative comparison between the values among materials containing Eu²⁺, Gd³⁺, or Tb⁴⁺ is available only in pairs (e.g., Eu²⁺/Gd³⁺ or Gd³⁺/Tb⁴⁺ in related hosts/sites). The lack of close structural similarity, combined with a dependence on the local structure, makes it difficult to definitively determine the effect of the metal identity and highlights the importance of the close structural congeners in this work.

The two Gd complexes, 2-Gd³⁺ and 3-Gd³⁺, highlight the significant impact that associated counterions can have on the resultant spectrum. Both complexes have the same coordination environment but differ in the binding or sequestration of the potassium counterion. If the counterion were not associated with the structure in solution, then both compounds would be expected to give identical EPR spectra. However, the spectra are quite different, as is reflected by the Δ^8S value, which increases by ~ 4.5 times from 3-Gd³⁺ to 2-Gd³⁺. Insight into this difference can be gleaned from a comparison of the crystal structures of these two complexes. The $\Sigma_{109.5}$ value for 3-Gd³⁺ is 6.0°, meaning that the structure adopts a nearly tetrahedral geometry, while the 2-Gd structure has a $\Sigma_{109.5}$ of 28.4°. The large difference in $\Sigma_{109.5}$ values for these two complexes arises from the K⁺ counterion in 2-Gd³⁺ that is bound to the inner sphere and distorts the ligand field about Gd³⁺, while sequestration of the K⁺ counterion in 3-Gd³⁺ only minimally perturbs the ligand geometry via charge pairing. These metrics are useful because for an f^7 ion ($S = 7/2$; $L = 0$), in a perfect tetrahedron, there can be no ZFS. Therefore, one would expect that the closer to an ideal tetrahedron, the smaller the anisotropy that would be observed. This simplistic expectation is found to be true in a comparison of the measured ZFS parameters of 2-Gd³⁺ and 3-Gd³⁺. Importantly, the expected reduction in the observed ZFS with decreasing deviation from the ideal tetrahedral symmetry is not found for 4-Tb⁴⁺. This complex reveals the largest ZFS of the series despite the very small distortion from an ideal tetrahedron. This observation implicates the significant changes in the electronic structure of the Tb⁴⁺ ion in comparison to both Eu²⁺ and Gd³⁺. The high symmetry of the tetrakis(imidophosphorane) coordination is reflected in the ZFS of the Gd³⁺ and Eu²⁺ complexes being of smaller magnitude than even these ions in the Pb²⁺ site in PbWO₄, where the lanthanide ion is in octacoordination by tungstate oxygen atoms.^{69,70} This comparison highlights the significance of the relatively large ZFS in 4-Tb⁴⁺ in this coordination environment.

To understand the basis of the divergent properties of the Tb⁴⁺ ion and the link between the spectroscopic properties and electronic structure, a series of complete active space self-consistent-field (CASSCF) calculations was performed followed by N-electron valence perturbation theory to second order (NEVPT2) to account for the dynamic correlation.^{79–85} To gain insight into the differences in bonding across the series, the results of these calculations were analyzed in terms of ab initio ligand-field theory (AILFT).^{86–88} Specifically, the energies and AILFT parameters of the free ions Eu²⁺, Gd³⁺, and Tb⁴⁺ and a series of truncated models of 1-Eu²⁺, 2-Gd³⁺/3-Gd³⁺, and 4-Tb⁴⁺ (referred to as Eu^M, Gd^M, and Tb^M, respectively) were compared. The truncated models were optimized starting with the crystallographically determined atomic coordinates where all methyl groups more than four bonds from the metal center were replaced with hydrogen

atoms and all counterions were removed (Figure S21). This suite of calculations forms a convenient framework to systematically evaluate the interplay between bonding, interelectronic repulsion, and SOC. The goal of these calculations is not to reproduce the experimental ZFS values but rather to understand how the electronic structure changes across the series. The accurate calculation of ZFS parameters for $4f^7$ systems is extremely challenging because of the numerous excited states that mix via SOC into the ground state and make significant contributions to the phenomenologically observed ZFS. This scenario makes the quantitative determination of D extremely sensitive to the accuracy of the calculated excited-state energies, which, in turn, are extremely sensitive to the geometry. Given these caveats, it is unreasonable to assume that the truncated geometries will model the exact magnitude of a given observed ZFS. The focus is on the *trend* of the energetics and mixing of the sextet states as well as the effects of covalent interactions.

The definition and evaluation of the covalency is not unique, and trends are sensitive to the choice of method. Here, the covalency is considered to be a one-electron interaction that is analyzed in terms of the nephelauxetic reduction.^{86,87,89} This effect was originally used to explain why the SOC and electron repulsion parameters in coordination complexes were reduced compared to those of the free ion.^{90,91} The nephelauxetic reduction results from two effects. The first is termed “symmetry-restricted” and arises from orbital mixing, specifically dilution of the metal orbitals with ligand character. The second is the “central field” and results from the change in the radial extent of the f (or d) orbital wave functions because of complexation of the metal with a ligand. The central field covalency will contribute mostly to the reduction of interelectronic repulsion, while the symmetry-restricted covalency will manifest itself primarily in the reduction of the SOC constant, ζ .^{89,92}

Comparing the percent reduction of the SOC parameter, defined as $[100 \times (1 - \zeta/\zeta_{\text{free}})]$, across the series reveals that all three model complexes exhibit very little reduction, $\sim 1\%$ compared to the calculated free-ion value (note that the Tb^{4+} free-ion value is greater than that of Eu^{2+} because of its greater effective nuclear charge).⁹³ This limited change in the SOC parameter in the model complexes is not unanticipated given the small radial extent of the $4f$ orbitals in the lanthanide series. Importantly, we find that Tb^{M} has a slightly greater reduction than either Gd^{M} or Eu^{M} , which are nearly equal. To confirm this result, the same calculations were performed on the hypothetical series of $[\text{LnCl}_4]^{1-0/1+}$ complexes. In this much simpler ligand field, it is again found that the reduction of the SOC parameter for the Tb^{4+} ion is greatest, while the reductions in ζ for the Gd^{3+} and Eu^{2+} ions are smaller and essentially the same (Figure S20 and Table S23). It is important to note that the SOC constant is only mapped onto the CASSCF wave function and that, for now, evaluation of the effects of the dynamic correlation are not possible. However, as noted by Aravena and co-workers, because the goal is to evaluate the effects of covalency as a one-electron property, neglect of the dynamic correlations, a multielectron interaction, is not a limitation.⁸⁷ A similar analysis can be performed for reduction of the interelectronic repulsion. In this case, the CASSCF and CASSCF+NEVPT2 wave functions can be mapped onto the ligand-field model. Here, no trend in the reduction of the interelectronic repulsion is found across the series. However, inclusion of the dynamic correlation further

reduces the interelectronic repulsion parameters by $\sim 0.5\text{--}1\%$. Interestingly, in the hypothetical $[\text{LnCl}_4]^{1-0/1+}$ series, we again find that the reduction is approximately equal for Gd^{3+} and Eu^{2+} , while the Tb^{4+} model exhibits a larger reduction. Overall, our computational results suggest that both the symmetry-restricted and central field covalency are larger in Tb^{4+} than in the Gd^{3+} and Eu^{2+} compounds. This observation trends with the AILFT-calculated ligand-field splitting (Δ_{LF}), defined as the difference between the highest and lowest AILFT orbital, which increases across the series $\Delta_{\text{LF}} = 334, 438, \text{ and } 914 \text{ cm}^{-1}$ for $\text{Eu}^{\text{M}}, \text{Gd}^{\text{M}}, \text{ and } \text{Tb}^{\text{M}}$, respectively.

Because quantitative calculation of the ZFS parameters is not possible for this $4f^7$ series, the AILFT model can be used to gain insight into the origins of the ZFS. The largest contribution to the magnitude of the ZFS is from SOC between the ^8S ground state and excited states of the ^6P manifold and is proportional to $\zeta^2/E(^6\text{P}_i)$, where $E(^6\text{P}_i)$ is the energy difference between ^8S and one of the three ^6P excited states.^{58,89,92,94} The separation of the ^8S and ^6P states is predominately governed by the strength of the interelectronic repulsion that increases from Eu^{2+} to Tb^{4+} (Figure 4).

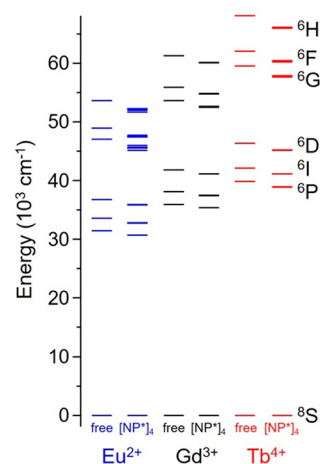


Figure 4. Energy levels for the ground ^8S state and excited sextet states calculated at the CASSCF/NEVPT2 level of theory. For each metal ion, the free ion and model structure energy levels are shown.

However, the calculations also show that the SOC constant increases from Eu^{2+} to Tb^{4+} . This increase in SOC means that the magnitude of the ZFS is a competition between the contributions from interelectronic repulsion and spin–orbit interactions. The ratio $\zeta^2/E(^6\text{P})$ increases across the series (Table 2) from Eu^{2+} to Tb^{4+} . This trend suggests that the contribution from the larger spin–orbit interaction in Tb^{4+} overwhelms that from the increased interelectronic repulsion and thus results in a larger ZFS. The trend of increasing $\zeta^2/$

Table 2. Metrics Derived from AILFT and CASSCF/NEVPT2 Calculations

	ζ (cm^{-1})	$\zeta/\zeta_{\text{free}}^a$	$E(^6\text{P})$ (cm^{-1})	$\zeta^2/E(^6\text{P})$	ground-state character	
					^8S (%)	^6P (%)
Eu^{M}	1259.5	0.989	30698.2	51.7	97.76	2.22
Gd^{M}	1545.9	0.991	35351.7	67.6	97.48	2.51
Tb^{M}	1848.1	0.987	38909.0	87.8	97.05	2.92

^a ζ_{free} values are calculated in this work and shown in the SI.

$E(^6P)$ from Eu^{2+} to Tb^{4+} is also reflected in the composition of the ground state that increases in 6P character upon moving from Eu^{2+} to Tb^{4+} (Table 2). This analysis demonstrates the competing interactions (SOC, interelectron repulsion, and ligand-field splitting) that lead Tb^{4+} to exhibit larger ZFS values than formally isoelectronic Eu^{2+} and Gd^{3+} . The ZFS is mostly determined by the splitting within the 6P state, e.g., in the T_d point group, and the microstates within P terms are triply degenerate, while in lower symmetry groups, this degeneracy is lifted. The magnitude of the splitting among these 6P microstates is then governed by the ligand-field strength. Because each of these microstates makes a different contribution to the ZFS, the computed ZFS values are extremely sensitive to the geometry of the molecule. This situation is particularly challenging because the magnitude of each individual contribution is often much larger than the ZFS. While these factors limit quantitative analysis of the experimental results, the significantly larger value of Δ^8S observed for the Tb complex is rationalized by the single-ion properties of the Tb^{4+} ion wherein the increased interelectronic repulsion, shown by the increased separation between the 8S and 6P states, is compensated for by a larger SOC interaction in Tb^{4+} .

CONCLUSION

The isolation of tetravalent terbium complexes facilitated the first ever series of isostructural, isoelectronic lanthanide complexes spanning three oxidation states. Despite an isotropic ground state (8S), conventional X-band EPR measurements of the tetravalent terbium compound in this study, as well as other tetravalent terbium complexes, exhibited strongly anisotropic spectra. The spectra contained broad, complex resonances, and using low-frequency EPR, the quantitative value of ZFS in these compounds was impossible to determine. Multifield fitting of the dc magnetometry data for all four compounds in this study highlights the increase in the ZFS (as given by Δ^8S , which gives the effect of ZFS without the complication of signage of traditional parameters) for Tb^{4+} compared to Eu^{2+} and Gd^{3+} in a nearly conserved ligand environment. This trend is replicated in the analysis of the solution and solid-state HF-EPR of the **1-Eu²⁺**, **2-Gd³⁺**, **3-Gd³⁺**, and **4-Tb⁴⁺** complexes, which demonstrate similar ZFS parameters for the Eu^{2+} and Gd^{3+} complexes. The Gd^{3+} parameters depend strongly on the deviation from tetrahedral coordination. As in the trend seen in the fit of the dc susceptibility data, the $|D|$ and Δ^8S values increase by ~ 8 times between **3-Gd³⁺** and **4-Tb⁴⁺**.

These experimental results were rationalized through CASSCF-NEVPT2 calculations on a series of model complexes (Eu^M , Gd^M , and Tb^M) and simplified tetrahedral structures ($[\text{LnCl}_4]^{1-0/1+}$ complexes). These calculations reveal that the similarity of the Eu^{2+} and Gd^{3+} single-ion properties and the divergence of the Tb^{4+} properties are driven by the competition between electron–electron repulsion and SOC. Specifically, in Tb^{4+} , the increase in the interelectronic repulsion is compensated for by a comparatively large increase in SOC (from Gd^{3+} to Tb^{4+} versus from Eu^{2+} to Gd^{3+}). Additionally, these studies contribute to the recent spectroscopic reevaluation^{95–97} of lanthanide covalent bonding and reveal that tetravalent lanthanides, even midlanthanides, have greater metal–ligand bond covalency than their di- and trivalent counterparts.

EXPERIMENTAL SECTION

General considerations are listed in the SI along with crystallographic information, magnetic data fits, EPR spectra, explicit strain model for EPR line width, and model geometries. The synthetic procedures for the reported compounds follow:

1-Eu²⁺. Inside a glovebox, $\text{EuI}_2(\text{THF})_2$ (0.246 g, 0.447 mmol) was added to a 20 mL scintillation vial charged with a glass stir bar and 2 mL of diethyl ether. $[\text{PN}^*]\text{K}$ (0.584 g, 1.79 mmol, 4.0 equiv) was added as a solution in diethyl ether (5 mL), and the reaction mixture was stirred overnight. The mixture was filtered through a fine-porosity frit packed with Celite. The filtrate was concentrated in vacuo to give an orange solid. The residue was triturated three times with 1 mL of *n*-pentane, then taken up in 5 mL of diethyl ether, and filtered through a pipet filter packed with Celite and glass filter paper. The dark-orange solution was concentrated in vacuo and placed inside a -35 °C freezer overnight, during which time dark-orange crystals were obtained (0.531 g, 86%). No ^1H , ^{13}C , or ^{31}P NMR signals were observed. IR (cm^{-1}): ν 1266 (m), 1246 (m), 1204 (s), 1180 (m), 1147 (s), 1093 (s), 1076 (s), 1047 (m), 1023 (m), 969 (w), 911 (w), 866 (w), 795 (w), 705 (s), 680 (m), 614 (w). Elem anal. Found (calcd): C, 49.15 (50.37); H, 9.60 (9.64); N, 14.65 (14.69). Carbon was consistently low on multiple burns. X-ray diffraction (XRD)-quality crystals were grown from a concentrated solution of diethyl ether at -35 °C.

2-Gd³⁺. Inside a glovebox, $\text{GdI}_3(\text{THF})_{3.5}$ (0.313 g, 0.396 mmol) was added to a 20 mL scintillation vial charged with a stir bar and 2 mL of diethyl ether. $[\text{PN}^*]\text{K}$ (0.518 g, 1.58 mmol, 4.0 equiv) was added as a solution in diethyl ether (5 mL), and the reaction mixture was stirred overnight. The mixture was filtered through a fine-porosity frit packed with Celite. The filtrate was concentrated in vacuo to give a pale-tan solid. The residue was triturated three times with 1 mL of *n*-pentane, then taken up in 5 mL of diethyl ether, and filtered through a pipet filter packed with Celite and glass filter paper. The pale-orange solution was concentrated in vacuo and placed inside a -35 °C freezer overnight, during which time colorless crystals were obtained (0.407 g, 71%). No ^1H , ^{13}C , or ^{31}P NMR signals were observed. IR (cm^{-1}): ν 1266 (m), 1246 (m), 1217 (s), 1200 (s), 1171 (s), 1151 (s), 1113 (m), 1051 (m), 1031 (m), 977 (w), 928 (w), 866 (w), 795 (w), 725 (w), 692 (m), 626 (w). Elem anal. Found (calcd): C, 50.12 (49.97); H, 9.66 (9.59); N, 16.48 (16.65). XRD-quality crystals were grown from a concentrated solution of diethyl ether at -35 °C.

3-Gd³⁺. Inside a glovebox, **1-Gd³⁺** (0.164 g, 0.122 mmol) was added to a 20 mL scintillation vial charged with a stir bar and 2 mL of 1,2-dimethoxyethane. 2.2.2-Cryptand (0.046 g, 0.122 mmol) was added as a solution in 1,2-dimethoxyethane (2 mL), and the reaction was stirred overnight. The mixture was filtered through a fine-porosity frit packed with Celite. The volume of the solution was reduced to around 3 mL in vacuo, and crystals were grown through slow evaporation at room temperature. The solution was decanted, and the colorless crystals were dried in vacuo to give the title compound (0.165 g, 79%). No ^1H , ^{13}C , or ^{31}P NMR signals were observed. IR (cm^{-1}): ν 1258 (m), 1250 (m), 1217 (s), 1200 (s), 1180 (s), 1155 (m), 1134 (m), 1105 (m), 1080 (w), 1051 (m), 1023 (m), 977 (w), 952 (w), 923 (w), 866 (w), 795 (w), 688 (m). Elem anal. Found (calcd): C, 50.81 (51.60); H, 9.49 (9.60); N, 14.61 (14.64). Carbon was consistently low on multiple burns. XRD-quality crystals were grown from an evaporated solution of 1,2-dimethoxyethane at room temperature.

ASSOCIATED CONTENT

Supporting Information

The Supporting Information is available free of charge at <https://pubs.acs.org/doi/10.1021/acs.inorgchem.1c01062>.

General considerations along with crystallographic information, magnetic data fits, EPR spectra, explicit strain models for EPR line widths, and model geometries (PDF)

Accession Codes

CCDC 2050809–2050811 contain the supplementary crystallographic data for this paper. These data can be obtained free of charge via www.ccdc.cam.ac.uk/data_request/cif, or by emailing data_request@ccdc.cam.ac.uk, or by contacting The Cambridge Crystallographic Data Centre, 12 Union Road, Cambridge CB2 1EZ, UK; fax: +44 1223 336033.

AUTHOR INFORMATION**Corresponding Author**

Henry S. La Pierre – School of Chemistry and Biochemistry and Nuclear and Radiological Engineering Program, Georgia Institute of Technology, Atlanta, Georgia 30332-0400, United States; orcid.org/0000-0002-0895-0655; Email: hsl@gatech.edu

Authors

Thaige P. Gomba – School of Chemistry and Biochemistry, Georgia Institute of Technology, Atlanta, Georgia 30332-0400, United States

Samuel M. Greer – Los Alamos National Laboratory (LANL), Los Alamos, New Mexico 87545, United States

Natalie T. Rice – School of Chemistry and Biochemistry, Georgia Institute of Technology, Atlanta, Georgia 30332-0400, United States; orcid.org/0000-0002-6233-7958

Ningxin Jiang – School of Chemistry and Biochemistry, Georgia Institute of Technology, Atlanta, Georgia 30332-0400, United States

Joshua Telser – Department of Biological, Physical and Health Sciences, Roosevelt University, Chicago, Illinois 60605, United States; orcid.org/0000-0003-3307-2556

Andrew Ozarowski – National High Magnetic Field Laboratory (NHMFL), Florida State University, Tallahassee, Florida 32310, United States; orcid.org/0000-0001-6225-9796

Benjamin W. Stein – Los Alamos National Laboratory (LANL), Los Alamos, New Mexico 87545, United States; orcid.org/0000-0002-0366-5476

Complete contact information is available at: <https://pubs.acs.org/10.1021/acs.inorgchem.1c01062>

Author Contributions

†These authors contributed equally.

Notes

The authors declare no competing financial interest.

ACKNOWLEDGMENTS

This material is based upon work supported the U.S. Department of Energy, Office of Science, Office of Basic Energy Sciences, Heavy Element Chemistry Program, under Award DE-SC0019385. A portion of this work was performed at the NHMFL (ID P19275), which is supported by the National Science Foundation (Grant DMR-1644779) and the State of Florida. S.M.G. acknowledges support from a Director's Postdoctoral Fellowship (LANL-LDRD). S.M.G. and B.W.S. are supported by the U.S. Department of Energy, Office of Science, Office of Basic Energy Sciences, Heavy Element Chemistry Program (Grant 2020LANLE372) at LANL. LANL is managed by Triad National Security, LLC, for the NNSA of the U.S. Department of Energy (Contract 89233218CNA000001). Single-crystal X-ray diffraction experi-

ments were performed at the GT SC-XRD facility directed by Dr. John Bacsa.

REFERENCES

- (1) Gomba, T. P.; Ramanathan, A.; Rice, N. T.; La Pierre, H. S. The chemical and physical properties of tetravalent lanthanides: Pr, Nd, Tb, and Dy. *Dalton Trans.* **2020**, 49 (45), 15945–15987.
- (2) Piro, N. A.; Robinson, J. R.; Walsh, P. J.; Schelter, E. J. The electrochemical behavior of cerium(III/IV) complexes: Thermodynamics, kinetics and applications in synthesis. *Coord. Chem. Rev.* **2014**, 260, 21–36.
- (3) Evans, W. J.; Davis, B. L. Chemistry of Tris(pentamethylcyclopentadienyl) f-Element Complexes, (C₅Me₅)₃M. *Chem. Rev.* **2002**, 102 (6), 2119–2136.
- (4) Morss, L. R. Thermochemical properties of yttrium, lanthanum, and the lanthanide elements and ions. *Chem. Rev.* **1976**, 76 (6), 827–841.
- (5) Nocton, G.; Ricard, L. N-aromatic heterocycle adducts of bulky [1,2,4-(Me₃C)₃C₃H₂]₂Sm: synthesis, structure and solution analysis. *Dalton Trans.* **2014**, 43 (11), 4380–4387.
- (6) Cheisson, T.; Auffrant, A.; Nocton, G. η⁵–η¹ Switch in Divalent Phosphaytterbocene Complexes with Neutral Iminophosphoranyl Pincer Ligands: Solid-State Structures and Solution NMR ¹JYb–P Coupling Constants. *Organometallics* **2015**, 34 (22), 5470–5478.
- (7) Xémard, M.; Zimmer, S.; Cordier, M.; Goudy, V.; Ricard, L.; Clavaguéra, C.; Nocton, G. Lanthanidocenes: Synthesis, Structure, and Bonding of Linear Sandwich Complexes of Lanthanides. *J. Am. Chem. Soc.* **2018**, 140 (43), 14433–14439.
- (8) MacDonald, M. R.; Bates, J. E.; Fieser, M. E.; Ziller, J. W.; Furche, F.; Evans, W. J. Expanding Rare-Earth Oxidation State Chemistry to Molecular Complexes of Holmium(II) and Erbium(II). *J. Am. Chem. Soc.* **2012**, 134 (20), 8420–8423.
- (9) MacDonald, M. R.; Bates, J. E.; Ziller, J. W.; Furche, F.; Evans, W. J. Completing the Series of + 2 Ions for the Lanthanide Elements: Synthesis of Molecular Complexes of Pr²⁺, Gd²⁺, Tb²⁺, and Lu²⁺. *J. Am. Chem. Soc.* **2013**, 135 (26), 9857–9868.
- (10) Fieser, M. E.; MacDonald, M. R.; Krull, B. T.; Bates, J. E.; Ziller, J. W.; Furche, F.; Evans, W. J. Structural, Spectroscopic, and Theoretical Comparison of Traditional vs Recently Discovered Ln²⁺ Ions in the [K(2.2.2-cryptand)][(C₅H₄SiMe₃)₃Ln] Complexes: The Variable Nature of Dy²⁺ and Nd²⁺. *J. Am. Chem. Soc.* **2015**, 137 (1), 369–382.
- (11) Evans, W. J. Tutorial on the Role of Cyclopentadienyl Ligands in the Discovery of Molecular Complexes of the Rare-Earth and Actinide Metals in New Oxidation States. *Organometallics* **2016**, 35 (18), 3088–3100.
- (12) Fieser, M. E.; Palumbo, C. T.; La Pierre, H. S.; Halter, D. P.; Voora, V. K.; Ziller, J. W.; Furche, F.; Meyer, K.; Evans, W. J. Comparisons of lanthanide/actinide + 2 ions in a tris(aryloxy)arene coordination environment. *Chem. Sci.* **2017**, 8 (11), 7424–7433.
- (13) Huh, D. N.; Darago, L. E.; Ziller, J. W.; Evans, W. J. Utility of Lithium in Rare-Earth Metal Reduction Reactions to Form Non-traditional Ln²⁺ Complexes and Unusual [Li(2.2.2-cryptand)]¹⁺ Cations. *Inorg. Chem.* **2018**, 57 (4), 2096–2102.
- (14) Ryan, A. J.; Darago, L. E.; Balasubramani, S. G.; Chen, G. P.; Ziller, J. W.; Furche, F.; Long, J. R.; Evans, W. J. Synthesis, Structure, and Magnetism of Tris(amide) [Ln{N(SiMe₃)₂}]¹⁻ Complexes of the Non-traditional + 2 Lanthanide Ions. *Chem. - Eur. J.* **2018**, 24 (30), 7702–7709.
- (15) Goodwin, C. A. P.; Chilton, N. F.; Vettese, G. F.; Moreno Pineda, E.; Crowe, I. F.; Ziller, J. W.; Winpenny, R. E. P.; Evans, W. J.; Mills, D. P. Physicochemical Properties of Near-Linear Lanthanide(II) Bis(silylamide) Complexes (Ln = Sm, Eu, Tm, Yb). *Inorg. Chem.* **2016**, 55 (20), 10057–10067.
- (16) Heitmann, D.; Jones, C.; Mills, D. P.; Stasch, A. Low coordinate lanthanide(II) complexes supported by bulky guanidinato and amidinato ligands. *Dalton Trans.* **2010**, 39 (7), 1877–1882.
- (17) Arnold, P. L.; Cloke, F. G. N.; Nixon, J. F. The first stable scandocene: synthesis and characterisation of bis(η²-4,5-tri-tert-

butyl-1,3-diphosphacyclopentadienyl)scandium(II). *Chem. Commun.* **1998**, 7, 797–798.

(18) Hitchcock, P. B.; Lappert, M. F.; Maron, L.; Protchenko, A. V. Lanthanum Does Form Stable Molecular Compounds in the + 2 Oxidation State. *Angew. Chem., Int. Ed.* **2008**, 47 (8), 1488–1491.

(19) Bochkarev, M. N.; Fedushkin, I. L.; Fagin, A. A.; Petrovskaya, T. V.; Ziller, J. W.; Broomhall-Dillard, R. N. R.; Evans, W. J. Synthesis and Structure of the First Molecular Thulium(II) Complex: $[\text{TmI}_2(\text{MeOCH}_2\text{CH}_2\text{OMe})_3]$. *Angew. Chem., Int. Ed. Engl.* **1997**, 36 (1–2), 133–135.

(20) Bochkarev, M. N.; Fedushkin, I. L.; Dechert, S.; Fagin, A. A.; Schumann, H. $[\text{NdI}_2(\text{thf})_5]$, the First Crystallographically Authenticated Neodymium(II) Complex. *Angew. Chem., Int. Ed.* **2001**, 40 (17), 3176–3178.

(21) Bochkarev, M. N.; Fagin, A. A. A New Route to Neodymium(II) and Dysprosium(II) Iodides. *Chem. - Eur. J.* **1999**, 5 (10), 2990–2992.

(22) Jacquot, L.; Xémard, M.; Clavaguéra, C.; Nocton, G. Multiple One-Electron Transfers in Bipyridine Complexes of Bis(phospholyl) Thulium. *Organometallics* **2014**, 33 (15), 4100–4106.

(23) Nocton, G.; Ricard, L. Reversible C–C coupling in phenanthroline complexes of divalent samarium and thulium. *Chem. Commun.* **2015**, 51 (17), 3578–3581.

(24) Andrez, J.; Bozoklu, G.; Nocton, G.; Pécaut, J.; Scopelliti, R.; Dubois, L.; Mazzanti, M. Lanthanide(II) Complexes Supported by N,O-Donor Tripodal Ligands: Synthesis, Structure, and Ligand-Dependent Redox Behavior. *Chem. - Eur. J.* **2015**, 21 (43), 15188–15200.

(25) Xémard, M.; Goudy, V.; Braun, A.; Tricoire, M.; Cordier, M.; Ricard, L.; Castro, L.; Louyriac, E.; Kefalidis, C. E.; Clavaguéra, C.; Maron, L.; Nocton, G. Reductive Disproportionation of CO_2 with Bulky Divalent Samarium Complexes. *Organometallics* **2017**, 36 (23), 4660–4668.

(26) Cheisson, T.; Ricard, L.; Heinemann, F. W.; Meyer, K.; Auffrant, A.; Nocton, G. Synthesis and Reactivity of Low-Valent f-Element Iodide Complexes with Neutral Iminophosphorane Ligands. *Inorg. Chem.* **2018**, 57 (15), 9230–9240.

(27) Xémard, M.; Cordier, M.; Louyriac, E.; Maron, L.; Clavaguéra, C.; Nocton, G. Small molecule activation with divalent samarium triflate: a synergistic effort to cleave O_2 . *Dalton Trans.* **2018**, 47 (28), 9226–9230.

(28) Willauer, A. R.; Dabrowska, A. M.; Scopelliti, R.; Mazzanti, M. Structure and small molecule activation reactivity of a metal-silsesquioxane of divalent ytterbium. *Chem. Commun.* **2020**, 56 (63), 8936–8939.

(29) Toniolo, D.; Willauer, A. R.; Andrez, J.; Yang, Y.; Scopelliti, R.; Maron, L.; Mazzanti, M. CS_2 Reductive Coupling to Acetylenedithiolate by a Dinuclear Ytterbium(II) Complex. *Chem. - Eur. J.* **2019**, 25 (33), 7831–7834.

(30) Willauer, A. R.; Toniolo, D.; Fadaei-Tirani, F.; Yang, Y.; Laurent, M.; Mazzanti, M. Carbon dioxide reduction by dinuclear Yb(II) and Sm(II) complexes supported by siloxide ligands. *Dalton Trans.* **2019**, 48 (18), 6100–6110.

(31) Kelly, R. P.; Toniolo, D.; Tirani, F. F.; Maron, L.; Mazzanti, M. A tetranuclear samarium(II) inverse sandwich from direct reduction of toluene by a samarium(II) siloxide. *Chem. Commun.* **2018**, 54 (73), 10268–10271.

(32) Plesniak, M. P.; Just-Baringo, X.; Ortu, F.; Mills, D. P.; Procter, D. J. SmCpR2-mediated cross-coupling of allyl and propargyl ethers with ketoesters and a telescoped approach to complex cycloheptanols. *Chem. Commun.* **2016**, 52 (92), 13503–13506.

(33) Moutet, J.; Schleinitz, J.; La Droitte, L.; Tricoire, M.; Pointillart, F.; Gendron, F.; Simler, T.; Clavaguéra, C.; Le Guennic, B.; Cador, O.; Nocton, G. Bis-cyclooctatetraenyl Thulium(II): Highly Reducing Lanthanide Sandwich Single Molecule Magnets. *Angew. Chem., Int. Ed.* **2021**, 60, 6042.

(34) Xémard, M.; Cordier, M.; Molton, F.; Duboc, C.; Le Guennic, B.; Maury, O.; Cador, O.; Nocton, G. Divalent Thulium Crown Ether

Complexes with Field-Induced Slow Magnetic Relaxation. *Inorg. Chem.* **2019**, 58 (4), 2872–2880.

(35) Meihaus, K. R.; Fieser, M. E.; Corbey, J. F.; Evans, W. J.; Long, J. R. Record High Single-Ion Magnetic Moments Through $4f_n5d_1$ Electron Configurations in the Divalent Lanthanide Complexes $[(\text{C}_5\text{H}_4\text{SiMe}_3)_3\text{Ln}]^+$. *J. Am. Chem. Soc.* **2015**, 137 (31), 9855–9860.

(36) Woodruff, D. N.; Winpenny, R. E. P.; Layfield, R. A. Lanthanide Single-Molecule Magnets. *Chem. Rev.* **2013**, 113 (7), 5110–5148.

(37) Gould, C. A.; McClain, K. R.; Yu, J. M.; Groshens, T. J.; Furche, F.; Harvey, B. G.; Long, J. R. Synthesis and Magnetism of Neutral, Linear Metallocene Complexes of Terbium(II) and Dysprosium(II). *J. Am. Chem. Soc.* **2019**, 141 (33), 12967–12973.

(38) Zhang, W.; Muhtadi, A.; Iwahara, N.; Ungur, L.; Chibotaru, L. F. Magnetic Anisotropy in Divalent Lanthanide Compounds. *Angew. Chem., Int. Ed.* **2020**, 59 (31), 12720–12724.

(39) Chilton, N. F.; Goodwin, C. A. P.; Mills, D. P.; Winpenny, R. E. P. The first near-linear bis(amide) f-block complex: a blueprint for a high temperature single molecule magnet. *Chem. Commun.* **2015**, 51 (1), 101–103.

(40) Rice, N. T.; Su, J.; Gompa, T. P.; Russo, D. R.; Telser, J.; Palatinus, L.; Bacsa, J.; Yang, P.; Batista, E. R.; La Pierre, H. S. Homoleptic Imidophosphorane Stabilization of Tetravalent Cerium. *Inorg. Chem.* **2019**, 58 (8), 5289–5304.

(41) Rice, N. T.; Popov, I. A.; Russo, D. R.; Bacsa, J.; Batista, E. R.; Yang, P.; Telser, J.; La Pierre, H. S. Design, Isolation, and Spectroscopic Analysis of a Tetravalent Terbium Complex. *J. Am. Chem. Soc.* **2019**, 141 (33), 13222–13233.

(42) Rice, N. T.; Popov, I. A.; Russo, D. R.; Gompa, T. P.; Ramanathan, A.; Bacsa, J.; Batista, E. R.; Yang, P.; La Pierre, H. S. Comparison of tetravalent cerium and terbium ions in a conserved, homoleptic imidophosphorane ligand field. *Chem. Sci.* **2020**, 11 (24), 6149–6159.

(43) Willauer, A. R.; Palumbo, C. T.; Scopelliti, R.; Zivkovic, I.; Douair, I.; Maron, L.; Mazzanti, M. Stabilization of the Oxidation State + IV in Siloxide-Supported Terbium Compounds. *Angew. Chem., Int. Ed.* **2020**, 59 (9), 3549–3553.

(44) Palumbo, C. T.; Zivkovic, I.; Scopelliti, R.; Mazzanti, M. Molecular Complex of Tb in the + 4 Oxidation State. *J. Am. Chem. Soc.* **2019**, 141 (25), 9827–9831.

(45) Willauer, A. R.; Palumbo, C. T.; Fadaei-Tirani, F.; Zivkovic, I.; Douair, I.; Maron, L.; Mazzanti, M. Accessing the + IV Oxidation State in Molecular Complexes of Praseodymium. *J. Am. Chem. Soc.* **2020**, 142 (12), 5538–5542.

(46) Goldfarb, D.; Stoll, S. *EPR Spectroscopy*; eMagRes, 2017.

(47) Deblonde, G. J. P.; Sturzbecher-Hoehne, M.; Rupert, P. B.; An, D. D.; Illy, M.-C.; Ralston, C. Y.; Brabec, J.; de Jong, W. A.; Strong, R. K.; Abergel, R. J. Chelation and stabilization of berkelium in oxidation state + IV. *Nat. Chem.* **2017**, 9 (9), 843–849.

(48) Antonio, M. R.; Williams, C. W.; Soderholm, L. Berkelium redox speciation. *Radiochim. Acta* **2002**, 90 (12), 851–856.

(49) Cary, S. K.; Su, J.; Galley, S. S.; Albrecht-Schmitt, T. E.; Batista, E. R.; Ferrier, M. G.; Kozimor, S. A.; Mocko, V.; Scott, B. L.; Van Alstine, C. E.; White, F. D.; Yang, P. A series of dithiocarbamates for americium, curium, and californium. *Dalton Trans.* **2018**, 47 (41), 14452–14461.

(50) Sperling, J. M.; Warzecha, E. J.; Celis-Barros, C.; Sergentu, D.-C.; Wang, X.; Klamm, B. E.; Windorff, C. J.; Gaiser, A. N.; White, F. D.; Beery, D. A.; Chemey, A. T.; Whitefoot, M. A.; Long, B. N.; Hanson, K.; Kögerler, P.; Speldrich, M.; Zurek, E.; Autschbach, J.; Albrecht-Schönzart, T. E. Compression of curium pyrrolidinedithiocarbamate enhances covalency. *Nature* **2020**, 583 (7816), 396–399.

(51) Krzystek, J.; Ozarowski, A.; Telser, J. Multi-frequency, high-field EPR as a powerful tool to accurately determine zero-field splitting in high-spin transition metal coordination complexes. *Coord. Chem. Rev.* **2006**, 250 (17), 2308–2324.

(52) Hassan, A. K.; Pardi, L. A.; Krzystek, J.; Sienkiewicz, A.; Goy, P.; Rohrer, M.; Brunel, L. C. Ultrawide Band Multifrequency High-

Field EMR Technique: A Methodology for Increasing Spectroscopic Information. *J. Magn. Reson.* **2000**, *142* (2), 300–312.

(53) Telser, J.; Ozarowski, A.; Krzystek, J. High-frequency and -field electron paramagnetic resonance of transition metal ion (d block) coordination complexes. *Electron Paramagnetic Resonance*; The Royal Society of Chemistry: London, 2013; Vol. 23, pp 209–263.

(54) Telser, J. EPR Interactions – Zero-Field Splittings. *eMagRes.* **2017**, *6* (2), 207–234.

(55) Telser, J. EPR Interactions—Zero Field Splittings. In *EPR Spectroscopy: Fundamentals and Methods*; Goldfarb, D., Stoll, S., Eds.; John Wiley & Sons, Ltd.: Chichester, U.K., 2018; pp 29–63.

(56) Benmelouka, M.; Van Tol, J.; Borel, A.; Port, M.; Helm, L.; Brunel, L. C.; Merbach, A. E. A High-Frequency EPR Study of Frozen Solutions of Gd(III) Complexes: Straightforward Determination of the Zero-Field Splitting Parameters and Simulation of the NMRD Profiles. *J. Am. Chem. Soc.* **2006**, *128* (24), 7807–7816.

(57) Clayton, J. A.; Keller, K.; Qi, M.; Wegner, J.; Koch, V.; Hintz, H.; Godt, A.; Han, S.; Jeschke, G.; Sherwin, M. S.; Yulikov, M. Quantitative analysis of zero-field splitting parameter distributions in Gd(III) complexes. *Phys. Chem. Chem. Phys.* **2018**, *20* (15), 10470–10492.

(58) Newman, D. J.; Urban, W. Interpretation of S-state ion E.P.R. spectra. *Adv. Phys.* **1975**, *24* (6), 793–844.

(59) Raitsimring, A. M.; Astashkin, A. V.; Baute, D.; Goldfarb, D.; Poluektov, O. G.; Lowe, M. P.; Zech, S. G.; Caravan, P. Determination of the Hydration Number of Gadolinium(III) Complexes by High-Field Pulsed 17O ENDOR Spectroscopy. *ChemPhysChem* **2006**, *7* (7), 1590–1597.

(60) Attempts to prepare analogues of 1-Eu²⁺ with one or both of the potassium cations sequestered as outer-sphere cations in crypts or crowns uniformly resulted in the isolation of oxidized products.

(61) Yang, L.; Powell, D. R.; Houser, R. P. Structural variation in copper(I) complexes with pyridylmethylamide ligands: structural analysis with a new four-coordinate geometry index, τ_4 . *Dalton Trans.* **2007**, *9*, 955–964.

(62) Shannon, R. *Acta Crystallogr., Sect. A: Cryst. Phys., Diffr., Theor. Gen. Crystallogr.* **1976**, *32*, 751–767.

(63) Chilton, N. F.; Anderson, R. P.; Turner, L. D.; Soncini, A.; Murray, K. S. PHI: A powerful new program for the analysis of anisotropic monomeric and exchange-coupled polynuclear d- and f-block complexes. *J. Comput. Chem.* **2013**, *34* (13), 1164–1175.

(64) Stoll, S.; Schweiger, A. EasySpin, a comprehensive software package for spectral simulation and analysis in EPR. *J. Magn. Reson.* **2006**, *178* (1), 42–55.

(65) Azarkh, M.; Groenen, E. J. J. Simulation of multi-frequency EPR spectra for a distribution of the zero-field splitting. *J. Magn. Reson.* **2015**, *255*, 106–113.

(66) Abragam, A.; Bleaney, B. *Electron Paramagnetic Resonance of Transition Ions*; Clarendon Press, 1970.

(67) Vazhenin, V. A.; Artyomov, M. Y.; Potapov, A. P.; Chernyshev, V. A.; Fokin, A. V.; Serdtsev, A. V. Relaxation of the environment of Gd³⁺ and Eu²⁺ impurity ions in the Y₃Al₅O₁₂ garnet. *Phys. Solid State* **2017**, *59* (5), 967–972.

(68) Vazhenin, V. A.; Potapov, A. P.; Asatryan, G. R.; Uspenskaya, Y. A.; Petrosyan, A. G.; Fokin, A. V. High-spin europium and gadolinium centers in yttrium–aluminum garnet. *Phys. Solid State* **2016**, *58* (8), 1627–1633.

(69) Yeom, T. H.; Lee, S. H.; Choh, S. H.; Han, T. J.; Kim, T. H.; Ro, J. H. Electron paramagnetic resonance characterization of impurity Gd³⁺ ions in a PbWO₄ single crystal. *J. Appl. Phys.* **2003**, *94* (6), 3796–3799.

(70) Yeom, T. H.; Kim, I. G.; Lee, S. H.; Choh, S. H.; Kim, T. H.; Ro, J. H. Electron paramagnetic resonance study of the Eu²⁺ ion in a PbWO₄ single crystal. *J. Appl. Phys.* **2000**, *87* (3), 1424–1428.

(71) Baker, J. M.; Chadwick, J. R.; Garton, G.; Hurrell, J. P. E.p.r. and endor of Tb⁴⁺ in thoria. *Proc. R. Soc. Lon. Ser-A* **1965**, *286* (1406), 352–365.

(72) First-order perturbation theory gives this result, which for low rhombicity, $|E/D| < 0.1$, is accurate to better than 1% compared to an

exact calculation. The complete analysis, here assuming $D > 0$ and setting the lowest doublet ($m_S = \pm 1/2$) at $-SD - 37.5E^2/D$, gives the next doublet ($m_S = \pm 3/2$) at $-3D + 27.9E^2/D$, the next ($m_S = \pm 5/2$) at $D + 7.5E^2/D$, and the highest ($m_S = \pm 7/2$) at $7D + 2.1E^2/D$. For example, for 1-Eu²⁺, the maximum splitting is 0.596 cm⁻¹ from this equation, which is close to $\Delta^8S = 0.58$ cm⁻¹.

(73) Freidzon, A. Y.; Kurbatov, I. A.; Vovna, V. I. Ab initio calculation of energy levels of trivalent lanthanide ions. *Phys. Chem. Chem. Phys.* **2018**, *20* (21), 14564–14577.

(74) Kramida, A.; Ralchenko, Y.; Reader, J. (NIST ASD Team). *NIST Atomic Spectra Database*, version 5.8; National Institute of Standards and Technology: Gaithersburg, MD, 2020; DOI: DOI: 10.18434/T4W30F. Available: <https://physics.nist.gov/asd> [2020-12-30].

(75) Beck, D. R.; Domeier, E. Improved RCI techniques for treating 4f atoms and ions: Application to Gd IV energies. *Can. J. Phys.* **2009**, *87* (1), 75–81.

(76) Hutton, D. R.; Milne, R. J. Paramagnetic resonance of Tb⁴⁺ in zircon. *J. Phys. C: Solid State Phys.* **1969**, *2* (12), 2297–2300.

(77) Hansen, S.; Mosel, B. D.; Müller-Warmuth, W.; Fielding, P. E. EPR Studies of Tb⁴⁺ in Single Crystals of Zircon and Scheelite Structure Silicates and Germanates. *Z. Naturforsch., A: Phys. Sci.* **1996**, *51* (8), 885–894.

(78) Ebendorff-Heidepriem, H.; Ehrhart, D. Electron spin resonance spectra of Eu²⁺ and Tb⁴⁺ ions in glasses. *J. Phys.: Condens. Matter* **1999**, *11* (39), 7627–7634.

(79) Andersson, K.; Malmqvist, P. Å.; Roos, B. O. Second-order perturbation theory with a complete active space self-consistent field reference function. *J. Chem. Phys.* **1992**, *96* (2), 1218–1226.

(80) Andersson, K.; Malmqvist, P. Å.; Roos, B. O.; Sadlej, A. J.; Wolinski, K. Second-order perturbation theory with a CAS-SCF reference function. *J. Phys. Chem.* **1990**, *94* (14), 5483–5488.

(81) Malmqvist, P. Å.; Roos, B. O. The CAS-SCF state interaction method. *Chem. Phys. Lett.* **1989**, *155* (2), 189–194.

(82) Angeli, C.; Cimiraglia, R.; Evangelisti, S.; Leininger, T.; Malrieu, J.-P. Introduction of n-electron valence states for multi-reference perturbation theory. *J. Chem. Phys.* **2001**, *114* (23), 10252–10264.

(83) Angeli, C.; Cimiraglia, R.; Malrieu, J.-P. n-electron valence state perturbation theory: A spinless formulation and an efficient implementation of the strongly contracted and of the partially contracted variants. *J. Chem. Phys.* **2002**, *117* (20), 9138–9153.

(84) Angeli, C.; Cimiraglia, R.; Malrieu, J.-P. N-electron valence state perturbation theory: a fast implementation of the strongly contracted variant. *Chem. Phys. Lett.* **2001**, *350* (3), 297–305.

(85) Angeli, C.; Bories, B.; Cavallini, A.; Cimiraglia, R. Third-order multireference perturbation theory: The n-electron valence state perturbation-theory approach. *J. Chem. Phys.* **2006**, *124* (5), 054108.

(86) Jung, J.; Atanasov, M.; Neese, F. Ab Initio Ligand-Field Theory Analysis and Covalency Trends in Actinide and Lanthanide Free Ions and Octahedral Complexes. *Inorg. Chem.* **2017**, *56* (15), 8802–8816.

(87) Aravena, D.; Atanasov, M.; Neese, F. Periodic Trends in Lanthanide Compounds through the Eyes of Multireference ab Initio Theory. *Inorg. Chem.* **2016**, *55* (9), 4457–4469.

(88) Singh, S. K.; Eng, J.; Atanasov, M.; Neese, F. Covalency and chemical bonding in transition metal complexes: An ab initio based ligand field perspective. *Coord. Chem. Rev.* **2017**, *344*, 2–25.

(89) Neese, F.; Solomon, E. I. Interpretation and Calculation of Spin-Hamiltonian Parameters in Transition Metal Complexes. *Magnetism: Molecules to Materials IV* **2001**, 345–466.

(90) Ballhausen, C. J. *Introduction to Ligand Field Theory*; McGraw-Hill Book Company Inc., 1962.

(91) Jorgensen, C. K.; Pappalardo, R.; Schmidtke, H. H. Do the “Ligand Field” Parameters in Lanthanides Represent Weak Covalent Bonding? *J. Chem. Phys.* **1963**, *39* (6), 1422–1430.

(92) Neese, F.; Solomon, E. I. Calculation of Zero-Field Splittings, g-Values, and the Relativistic Nephelauxetic Effect in Transition Metal Complexes. Application to High-Spin Ferric Complexes. *Inorg. Chem.* **1998**, *37* (26), 6568–6582.

(93) The NIST Atomic Spectra Database Levels Data^{73,74} gives extensive information on free ion Eu^{2+} , minimal on Gd^{3+} , and none on Tb^{3+} . Thus, a direct comparison of the trends observed here for imidophosphorane complexes with the free ions is not possible. It is clear, however, that the ${}^6\text{P}$ first excited state is closer in energy to the ${}^8\text{S}$ ground state in Eu^{2+} than in Gd^{3+} (by $\sim 10 - 15\%$), which is consistent with the results in Table 2. The ground-state character calculated here (Table 2) as $\sim 97\%$ ${}^8\text{S}$ and $\sim 3\%$ ${}^6\text{P}$ is also consistent with the free-ion results.

(94) Atanasov, M.; Aravena, D.; Suturina, E.; Bill, E.; Maganas, D.; Neese, F. First principles approach to the electronic structure, magnetic anisotropy and spin relaxation in mononuclear 3d-transition metal single molecule magnets. *Coord. Chem. Rev.* **2015**, *289–290*, 177–214.

(95) Löble, M. W.; Keith, J. M.; Altman, A. B.; Stieber, S. C. E.; Batista, E. R.; Boland, K. S.; Conradson, S. D.; Clark, D. L.; Lezama Pacheco, J.; Kozimor, S. A.; Martin, R. L.; Minasian, S. G.; Olson, A. C.; Scott, B. L.; Shuh, D. K.; Tyliczszak, T.; Wilkerson, M. P.; Zehnder, R. A. Covalency in Lanthanides. An X-ray Absorption Spectroscopy and Density Functional Theory Study of LnCl_6^{x-} ($x = 3, 2$). *J. Am. Chem. Soc.* **2015**, *137* (7), 2506–2523.

(96) Su, J.; Batista, E. R.; Boland, K. S.; Bone, S. E.; Bradley, J. A.; Cary, S. K.; Clark, D. L.; Conradson, S. D.; Ditter, A. S.; Kaltsoyannis, N.; Keith, J. M.; Kerridge, A.; Kozimor, S. A.; Löble, M. W.; Martin, R. L.; Minasian, S. G.; Mocko, V.; La Pierre, H. S.; Seidler, G. T.; Shuh, D. K.; Wilkerson, M. P.; Wolfsberg, L. E.; Yang, P. Energy-Degeneracy-Driven Covalency in Actinide Bonding. *J. Am. Chem. Soc.* **2018**, *140* (51), 17977–17984.

(97) Minasian, S. G.; Batista, E. R.; Booth, C. H.; Clark, D. L.; Keith, J. M.; Kozimor, S. A.; Lukens, W. W.; Martin, R. L.; Shuh, D. K.; Stieber, S. C. E.; Tyliczszak, T.; Wen, X.-d. Quantitative Evidence for Lanthanide-Oxygen Orbital Mixing in CeO_2 , PrO_2 , and TbO_2 . *J. Am. Chem. Soc.* **2017**, *139* (49), 18052–18064.